Anal. Chem. **2003,** *75,* 6223−6230

Characterization of Gas-Phase Adsorption on Metal Oxide Thin Films Using a Magnetoelastic Resonance Microbalance

Michael E. Zorn,*,†,§ Kari A. Rahne,† M. Isabel Tejedor-Tejedor,† Marc A. Anderson,† and Craig A. Grimes‡

Environmental Chemistry and Technology Program, University of Wisconsin−Madison, 660 North Park Street, Madison, Wisconsin 53706, and Department of Electrical Engineering, and Department of Materials Science and Engineering, Penn State University, 217 Materials Research Laboratory, University Park, Pennsylvania 16802

In this study, a magnetoelastic resonance microbalance (MERM) was used to directly measure the gas-phase adsorption behavior of water vapor, isopropyl alcohol, and acetone on a sol−gel-derived titanium dioxide sensor coating. The nature of the MERM platform enables chemical measurements in situations in which wires or physical connections are undesired (or not possible) or in which sensor cost is a major issue. The underlying MERM technique (with an uncoated sensor) showed excellent day-to-day stability, a linear calibration over a 1 kHz change in frequency (or a 1.5-mg change in mass), and the ability to detect a mass change of 15 *μ*g without any efforts at sensitivity optimization. The titanium dioxide coated sensor yielded excellent response to each of the analytes; however, the response did not follow a simple linear calibration function. A more complex calibration model or utilization of the coated sensor in a limited concentration range would be required for quantitative analysis. The process of applying the metal oxide coatings onto the magnetic substrate altered the structure of the thin film layer, resulting in a relatively loose packing of the porous primary titanium dioxide particles to create an open overall honeycomb structure, thereby affecting the adsorption behavior at high relative concentration.

Amorphous, ferromagnetic magnetoelastic thick-film ribbons form an extraordinarily versatile method for detecting small changes in mass, enabling their use as sensors. In response to a time-varying magnetic field, these ribbons efficiently convert magnetic energy into mechanical energy. A magnetic field impulse, ≈4 A/m, is used to impart elastic energy into a magnetoelastic sensor, which in turn acts to mechanically strain the material in a transitory, time decaying, response. Since the material is also magnetostrictive, the deformed sensor generates magnetic flux that extends remotely about the device. The magnetoelastic sensor magnetically "rings" at its resonance frequency (f_0), which can rapidly (<1 ms) be detected using a pickup coil and microprocessor-based frequency counting techniques. An important feature of these systems is that no direct physical connections to the sensor are required, nor is an internal power source (i.e., a battery) required for sensor operation.

An applied mass load (Δm) that is small in comparison to the mass of the sensor (m_0), will result in a corresponding decrease in the resonant frequency Δf. A simple relationship is given as[1,2]

$$\Delta f = -f_0 \frac{\Delta m}{2m_0} \tag{1}$$

Tracking changes in the measured resonant frequency enables determination of applied mass loads; hence, the magnetoelastic sensor platform can be considered a magnetoelastic resonance microbalance, or MERM. Figure 1 is a schematic that illustrates the operational principle of a MERM system.

Although magnetoelastic sensors have long been used as markers for electronic article surveillance,[3] tracking changes in the resonance frequency of a magnetoelastic sensor enables the determination of other variables. Magnetoelastic sensors have been used to measure physical parameters, such as temperature,[4] pressure,[5,6] liquid viscosity and density,[7] and magnetic field strength.[8] They have also been used as position sensors[9] and strain sensors.[10,11] A recent review provides a more complete list of examples.[12] Magnetoelastic sensors can also be used as chemical or biological sensors when combined with a layer that changes

* Corresponding author. Phone: 920-465-5758. E-mail: zornm@uwgb.edu.
† University of Wisconsin−Madison.
‡ Penn State University.
§ Present address: Department of Natural and Applied Sciences (Chemistry), University of Wisconsin−Green Bay, 2420 Nicolet Drive, Green Bay, WI 54311.

(1) Grimes, C. A.; Ong, K. G.; Loiselle, K.; Stoyanov, P. G.; Kouzoudis, D.; Liu, Y.; Tong, C.; Tefiku, F. *Smart Mater. Struct.* **1999**, *8*, 639−46.
(2) Schmidt, S.; Grimes, C. A. *Sens. Actuators, A* **2001**, *94*, 189−96.
(3) Ryan, J. *Sci. Am.* **1997**, *276*, 120.
(4) Jain, M. K.; Schmidt, S.; Ong, K. G.; Mungle, C.; Grimes, C. A. *Smart Mater. Struct.* **2000**, *9*, 502−10.
(5) Grimes, C. A.; Kouzoudis, D. *Sens. Actuators, A* **2000**, *84*, 205−12.
(6) Jain, M. K.; Cai, Q. Y.; Grimes, C. A. *Smart Mater. Struct.* **2001**, *10*, 347−53.
(7) Grimes, C. A.; Kouzoudis, D.; Mungle, C. *Rev. Sci. Instrum.* **2000**, *71*, 3822−24.
(8) Mohri, K.; Takeuchi, S. *J. Appl. Phys.* **1982**, *53*, 8386−88.
(9) Barandiaran, J. M.; Gutierrez, J. *Sens. Actuators, A* **1997**, *59*, 38−42.
(10) Mitchell, E. E.; DeMoyer, R.; Vranish, J. *IEEE Trans. Ind. Elec.* **1986**, *IE-33*, 166−70.
(11) Kouzoudis, D.; Grimes, C. A. *Smart Mater. Struct.* **2000**, *9*, 885−89.
(12) Grimes, C. A.; Mungle, C. S.; Zeng, K.; Jain, M. K.; Dreschel, W. R.; Paulose, M.; Ong, K. G. *Sensors* **2002**, *2*, 289−308.

10.1021/ac034273z CCC: $25.00
Published on Web 09/26/2003

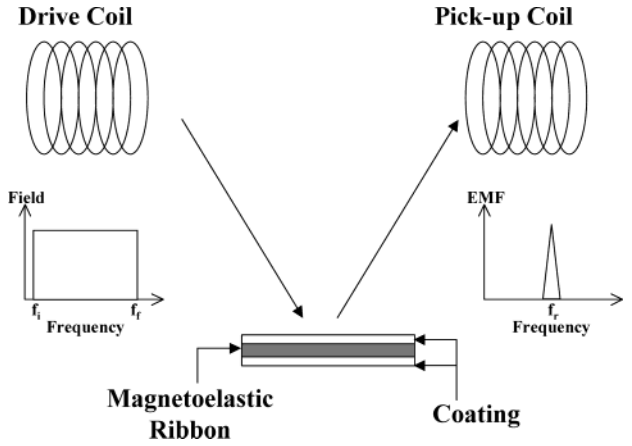

Figure 1. General schematic of the magneto elastic resonance microbalance (MERM) used in this study. Magnetoelastic sensors of this size can be monitored from a distance of ~50 cm; larger sensors provide more signal, enabling them to be monitored over greater distances.

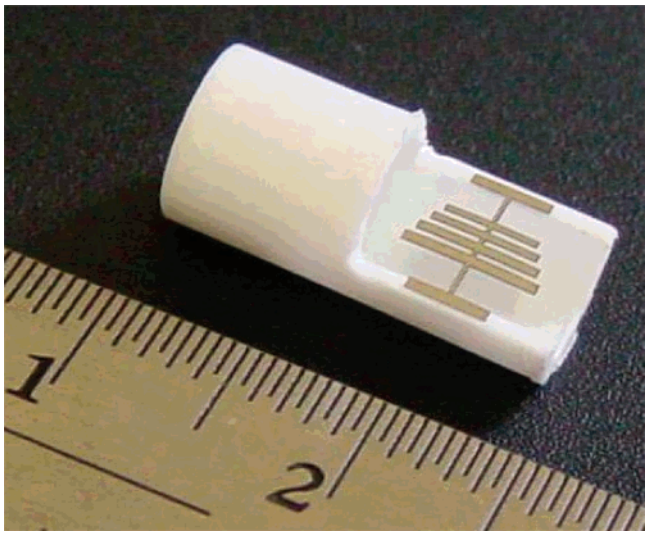

Figure 2. A four-element magnetoelastic sensor array, defined using a laser-cutting tool from a continuous ribbon, for simultaneous multiparameter environmental monitoring. The tabs at the top and bottom of the array are used for sensor mounting. The major scale of the ruler is centimeters. The smaller sensor in the array, far right, is ~28 μm × 250 μm × 3.5 mm in size.

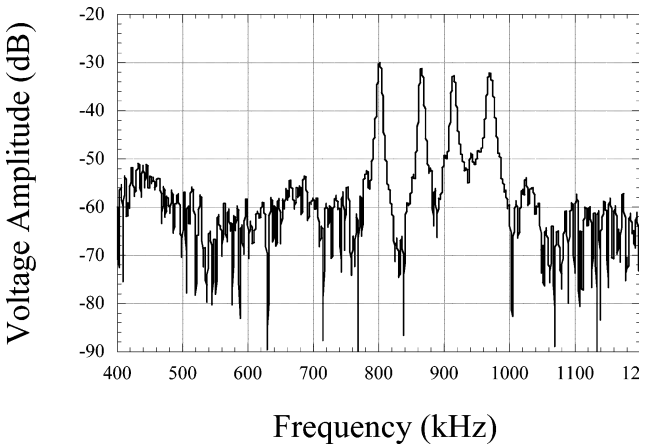

Figure 3. The frequency spectrum of the four-element sensor platform shown in Figure 2. The response of each sensor is independent, allowing for simultaneous multiparameter sensing.

mass or elasticity in response to an analyte of interest. Magnetoelastic-based sensors have successfully been use to monitor different gas analytes, including humidity,[4,5,13] ethylene,[14] ammonia,[15] and carbon dioxide,[16] as well as aqueous chemicals, including pH,[6,17] salt, and glucose concentrations.[12]

There are several advantages of magnetoelastic sensors over similar mass-based sensor platforms, such as surface acoustic wave (SAW) sensors or quartz crystal microbalances (QCMs).[18,19] As mentioned above, no direct physical connections to the sensor are required, nor is an internal power source (i.e., a battery) required for sensor operation. Although the competing technologies exhibit similar sensitivity to target analytes, magnetoelastic sensors cost ~10^4 less than surface acoustic wave sensors (absolute numbers depend on sensor size and frequency). Magnetoelastic ribbons, available from Honeywell Corporation (Morristown, NJ), have a material cost of approximately $200/km. This factor becomes a major issue if the sensors are needed on a single-use basis. In addition, the small footprint of the magnetoelastic sensor arrays makes them ideally suited for use within the nodes of sensor networks where constraints of space and power are at a premium. Therefore, magnetoelastic sensors make practical a highly accurate, miniature, mass/elasticity-based sensor technology inexpensive enough to be readily used on a disposable basis.

In addition, simultaneous tracking and cross-correlating the response of multiple magnetoelastic sensors enables absolute determination of multiple parameters in a complex environment. Figure 2 shows a four-sensor magnetoelastic sensor array (laser-cut from a 1.0 cm × 28 μm continuous ribbon) used for simultaneous measurement of humidity, CO_2, temperature and pressure. A frequency spectrum from this sensor array is shown in Figure 3. Recent developments in electronics[20] have demonstrated the ability to monitor a magnetoelastic sensor array, such as that shown in Figure 2, from a distance of ~50 cm; larger sensors provide more signal, enabling them to be monitored over greater distances.

The majority of previous chemical measurements using magnetoelastic sensors have utilized polymer-based coatings;[15,16] however, it is also possible to utilize inorganic ceramic materials as the analyte-responsive layer.[13] Sol−gel processing is a versatile fabrication method that employs the controlled hydrolysis of a metal alkoxide or metal salt to prepare a stable colloidal suspension, or sol.[21,22] Temperature, pH, ratio of water to metal alkoxide precursor, incorporation of a secondary solvent, size of alkyl

(13) Grimes, C. A.; Kouzoudis, D.; Dickey, E. C.; Qian, D.; Anderson, M. A.; Shahidain, R.; Lindsey, M.; Green, L. *J. Appl. Phys.* **2000**, *87*, 5341−43.
(14) Zhang, R.; Tejedor, M. I.; Anderson, M. A.; Paulose, M.; Grimes, C. A. *Sensors* **2002**, *2*, 331−38.
(15) Cai, Q. Y.; Jain, M. K.; Grimes, C. A. *Sens. Actuators, B* **2001**, *77*, 614−19.
(16) Cai, Q. Y.; Cammers-Goodwin, A.; Grimes, C. A. *J. Environ. Monit.* **2000**, *2*, 556−60.
(17) Cai, Q. Y.; Grimes, C. A. *Sens. Actuators, B* **2001**, *79*, 144−49.
(18) Grate, J. W.; Martin, S. J.; White, R. M. *Anal. Chem.* **1993**, *65*, A940−A948.
(19) Grate, J. W.; Martin, S. J.; White, R. M. *Anal. Chem.* **1993**, *65*, A987−A996.
(20) Zeng, K. F.; Ong, K. G.; Mungle, C.; Grimes, C. A. *Rev. Sci. Instrum.* **2002**, *73*, 4375−80.
(21) Brinker, C. J.; Scherer, G. W. *Sol−gel science: the physics and chemistry of sol−gel processing*; Academic Press: San Diego, CA, 1990.

groups on the metal alkoxide, and reaction kinetics are all important factors that together control the size of the primary particles formed from hydrolysis.[23] These stable colloidal sols can be coated onto a variety of substrates and fired to form a thin film[24−28] or a microporous ceramic membrane.[29−31] Pore size and porosity of the films can be tailored by controlling particle size and particle packing.[23] It is also possible to alter the surface chemistries by adding adsorbates to the suspensions to change the nature of the particle surface or by doping the final microporous materials with specific adsorbates.[28,32−34]

The purpose of this paper is to demonstrate the use of a MERM as a means of measuring the gas-phase adsorption behavior of several test analytes (i.e., water, isopropyl alcohol, and acetone) on a metal oxide (TiO_2) thin film sensor coating by directly measuring the surface concentration of the analyte. Characterization of the gas-phase adsorption behavior of an analyte is a critical step in the evaluation of a particular coating's effectiveness as a gas sensor. More specifically, it is the combined response of the magnetoelastic ribbon and the sensing film that will eventually be correlated (via a calibration curve) to the gas-phase concentration in a working sensor. Previous attempts to characterize the adsorption behavior of gas-phase compounds on sol−gel derived materials have mainly been limited to nondirect methods, in which adsorption is determined by comparison between the measured and expected gas-phase concentration.[35] The main advantage of direct measurements over indirect methods is an increased sensitivity, especially where adsorption by other components in the system (e.g., glass or metal surfaces) is nonnegligible.

EXPERIMENTAL SECTION

Magnetoelastic Resonance Microbalance. The electronic components used to generate the magnetic interrogation signal and to detect the emitted magnetoelastic signal are a function of the frequency range in which the sensors operate, which are in turn dependent upon the physical size of the sensors. In this work, magnetoelastic sensors having a nominal length of 4.0 cm, with an unloaded characteristic resonance frequency of ≈59.0 kHz were used. The computer-controlled MERM instrument utilized a Wavetek function generator to generate the interrogation signal, which was subsequently amplified by a Mackie power amplifier. The output from the amplifier was passed to a coil that was used to generate the magnetic interrogation field; in this work, a Helmholtz coil configuration was used, with a 16-turn coil of radius 15 cm, generating an interrogation field amplitude of ≈50 mOe. The magnetoelastic ribbon was tuned to its optimal operating point (maximum amplitude) by application of a DC magnetic biasing field (DC power supply: BOP 50-2M, Kepco, Inc., Flushing, NY) of ∼4 Oe intensity to overcome the anisotropy field of the ribbon. The DC field can also be applied by adjacent placement of a thick-film magnet. The resulting magnetic flux change of the magnetoelastic ribbon was detected using a closely placed pickup coil, the output of which is fed into a lock-in amplifier (SR 830 DSP, Stanford Research Systems, Sunnyvale, CA). The output of the lock-in amplifier was collected by the computer to provide the amplitude−frequency spectrum of the sensor, further enabling determination of resonance frequency and resonance quality factor (Q).

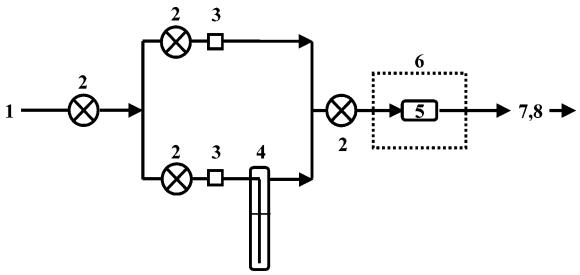

Figure 4. Experimental setup for the MERM adsorption measurements. 1, ultrahigh-purity nitrogen feed stream; 2, flow controllers; 3, check valves; 4, saturator with liquid water, acetone, or isopropyl alcohol; 5, adsorption chamber containing a titanium dioxide-coated magnetic ribbon; 6, magnetically active area containing interrogation and pickup coils; 7, relative humidity meter; and 8, volumetric flow meter.

The magnetic ribbons utilized in this study consisted of Metglas 2826 alloy MB ($Fe_{40}Ni_{38}Mo_4B_{18}$); the ribbons were 38.1 mm long × 12.7 mm wide × 30.5 μm thick in size. The magnetic ribbons (coated as described below) were housed in a 2.5-cm-i.d. × 4.0-cm-long borosilicate glass flow-through adsorption chamber that was fitted with Teflon end caps; other than the inlet and outlet connections, this chamber was gastight with respect to the ambient environment. The magnetic ribbons were placed on a Teflon platform inside the chamber, and the chamber was wrapped with several layers of Teflon tape to exclude ambient light. The chamber was then integrated into the overall experimental setup, as shown in Figure 4. The configuration allowed for removal of the adsorption chamber from the magnetically active area, followed by placement into a small heating compartment (and vice versa) without the interruption of gas flow. Unless otherwise specified, 50 data points were collected for each sample over a 200-Hz scan range that included the resonant frequency. Each reported frequency was an average of three successive scans. An example of the output from two separate scans is given in Figure 5. The two peaks in this example are separated by 29.9 Hz, or an approximate mass of 0.051 mg (as measured by the MERM), with a measurement error of ±1 Hz.[20]

(22) Pierre, A. C. *Introduction to sol−gel processing*; Kluwer Academic Publishers: Boston, 1998.
(23) Xu, Q. Y.; Anderson, M. A. *J. Mater. Res.* **1991**, *6*, 1073−81.
(24) Zorn, M. E.; Tompkins, D. T.; Zeltner, W. A.; Anderson, M. A. *Appl. Catal., B* **1999**, *23*, 1−8.
(25) Miller, L. W.; Tejedor-Tejedor, M. I.; Anderson, M. A. *Environ. Sci. Technol.* **1999**, *33*, 2070−75.
(26) Sirisuk, A.; Hill, C. G.; Anderson, M. A. *Catal. Today* **1999**, *54*, 159−64.
(27) Nelson, B. P.; Candal, R.; Corn, R. M.; Anderson, M. A. *Langmuir* **2000**, *16*, 6094−101.
(28) Zorn, M. E.; Tompkins, D. T.; Zeltner, W. A.; Anderson, M. A. *Environ. Sci. Technol.* **2000**, *34*, 5206−10.
(29) Peterson, R. A.; Anderson, M. A.; Hill, C. G. *J. Membr. Sci.* **1994**, *94*, 103−09.
(30) Peterson, R. A.; Webster, E. T.; Niezyniecki, G. M.; Anderson, M. A.; Hill, C. G. *Sep. Sci. Technol.* **1995**, *30*, 1689−709.
(31) Vichi, F. M.; Colomer, M. T.; Anderson, M. A. *Electrochem. Solid-State Lett.* **1999**, *2*, 313−16.
(32) Fu, X. Z.; Clark, L. A.; Zeltner, W. A.; Anderson, M. A. *J. Photochem. Photobiol,. A* **1996**, *97*, 181−86.
(33) Vichi, F. M.; Tejedor-Tejedor, M. I.; Anderson, M. A. *Chem. Mater.* **2000**, *12*, 1762−70.
(34) Sibu, C. P.; Kumar, S. R.; Mukundan, P.; Warrier, K. G. K. *Chem. Mater.* **2002**, *14*, 2876−81.
(35) Coronodo, J. M.; Zorn, M. E.; Tejedor-Tejedor, M. I.; Anderson, M. A. *Appl. Catal., B* **2003**, *43*, 329−44.

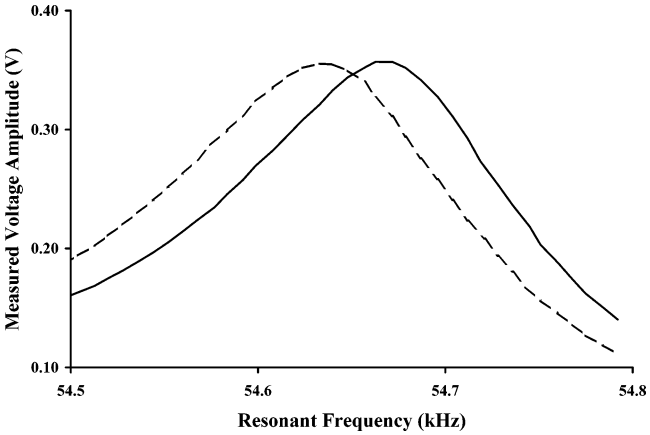

Figure 5. Sample MERM response peaks. The resonant frequency corresponds to the maximum MERM response. The two peaks in this example are separated by 29.9 Hz, or an approximate mass of 0.051 mg (using a calibration factor of 590.64 Hz mg^{-1}).

MERM Characterization. Initial experiments were performed to evaluate the MERM for reproducibility and day-to-day stability. Prior to testing, an uncoated ribbon was preconditioned by heating to 150 °C for 2 h in air. The ribbon was placed in the flow-through chamber and exposed to a stream of ultrahigh-purity (UHP) nitrogen (<2 ppm water, <1 ppm oxygen, <1 ppm total hydrocarbons, AGA Specialty Gas, Cleveland, OH) that was maintained at a flow rate of between 275 and 280 mL min^{-1} at a laboratory temperature of 21 °C ± 0.5 °C. The resonant frequency of this ribbon was then periodically monitored for 9 days; a total of 45 individual measurements were collected. Over the course of a given day, subsequent measurements were collected for a minimum of 1 h and a maximum of 6 h; all components were turned off, and N_2 flow was terminated at the end of a given day.

MERM Mass Calibration. The relationship between the change in resonant frequency and the change in mass of the magnetoelastic ribbons was evaluated to calibrate the MERM and to confirm linearity. Resonant frequency and ribbon mass were measured (using the MERM and an analytical balance, respectively) before and after sputtering several ribbons with platinum metal. The platinum layer was deposited as a protective barrier prior to exposing the ribbons to the slightly acidic titania sols (see below). The platinum (99.99% purity) was deposited using a cold sputtering device (model DESK II, Denton Vacuum, LLC, Moorestown, NJ) maintained at a current of 45 mA and a pressure of 50 mTorr argon. For this experiment, sputtering conditions were varied to deposit variable quantities of platinum onto the ribbons.

Thin Film Coatings. Stable sols of titanium dioxide (TiO_2) nanoparticles were prepared following the original method of Xu and Anderson.[23] In this method, titanium tetraisopropoxide ($Ti(OPr^i)_4$) (Aldrich, Milwaukee, WI) was subjected to an acidic hydrolysis by addition to an aqueous solution of nitric acid at a volumetric mixing ratio of 1 HNO_3/136.4 H_2O/11.4 $Ti(OPr^i)_4$. The resulting white TiO_2 precipitate was peptized at room temperature for 3 days, resulting in a stable suspension (sol). This acidic sol was then dialyzed for 3 days (Spectra/Por 3 membrane, 3500 MW cutoff, Spectrum, Laguna Hills, CA) to a final pH of 3.5.

For the adsorption studies, five identical magenetic ribbons were utilized. The ribbons were first coated on both sides with a protective layer of platinum metal to avoid corrosion of the bulk metal alloy. The platinum was deposited using the cold sputtering device described above, with an exposure time of 450 s. These conditions were sufficient to apply an average of 0.7 mg of Pt metal per ribbon, or 0.07 mg of Pt cm^{-2} of geometric surface area. The data derived from this procedure were also used to recalibrate the MERM prior to conducting the adsorption experiments. The platinized ribbons were then coated with a stable TiO_2 sol prepared as described above. Three layers were deposited by dip-coating at a withdrawal rate of 6 cm min^{-1} under a controlled humidity (20% RH) environment. After applying each layer, the ribbons were allowed to dry at 20% relative humidity for ~15 min before applying the subsequent layer. The coated ribbons were then fired in air in a furnace at 300 °C for 3 h using a 3 °C min^{-1} ramp rate. Previous studies have shown that the primary form of these titania materials fired at 300 °C is anatase (~80−90%),[32,36] and the specific surface area and porosity of similarly prepared titania particulates is 200 m^2 g^{-1} and 50%, respectively.[37] An average mass of 0.6 mg TiO_2 was deposited on the ribbons using this procedure, as determined by weighing with a laboratory balance after heating and without exposure to the ambient laboratory environment; individual measurements ranged between 0.4 and 0.8 mg TiO_2.

Adsorption Studies. The adsorption behavior of the TiO_2-coated magnetic ribbons was evaluated with three test analytes (water vapor, isopropyl alcohol vapor, and acetone vapor) using the MERM. Immediately prior to conducting each experiment, a coated magnetic ribbon was preconditioned (to remove physisorbed water) by heating in the adsorption chamber for a minimum of 2 h at 100 °C under a stream of UHP nitrogen that was maintained at a constant flow rate of 250 mL min^{-1}. Without removing the ribbon from the adsorption chamber or interrupting the nitrogen flow, the coated ribbon was subsequently cooled to room temperature for a minimum of 1 h (to allow for complete temperature equilibration), and the adsorption chamber was placed inside the magnetically active area. The resonant frequency was then measured under flowing nitrogen in the absence of analyte.

The analyte was then introduced into the feed stream by directing a portion of the nitrogen flow through a liquid saturator, as shown in Figure 4.By changing the relative flow through each fraction, the gas-phase analyte concentration could be controlled. Water vapor and organic solvent vapor (acetone and isopropyl alcohol) concentrations were monitored using a humidity meter (model HM34, Vaisala, Woburn, MA) and gas chromatograph (GC, Hewlett-Packard 5890 series II with FID detection and a Porapak R packed column from Alltech Associates, Deerfield, IL), respectively. Prior to measuring the resonant frequency at a given analyte concentration, a minimum equilibration period of 15 min was provided. Equilibration at a given condition was verified by monitoring the resonant frequency until no measurable change was observed.

To better understand the adsorption behavior, the MERM response was re-expressed in terms of the analyte surface concentration. Analyte surface concentration (Γ, in units of mmol g^{-1}) was calculated using the following equation

(36) Fu, X. Z.; Zeltner, W. A.; Anderson, M. A. *Appl. Catal., B* **1995**, *6*, 209−24.
(37) Fu, X. Z.; Clark, L. A.; Yang, Q.; Anderson, M. A. *Environ. Sci. Technol.* **1996**, *30*, 647−53.

$$\Gamma = \frac{-\Delta f}{K_{\mathrm{MERM}} MW} \qquad (2)$$

where $\Delta f = f$ in the presence of analyte minus f under dry conditions (in units of Hz), K_{MERM} is the MERM calibration factor (in units of Hz mg^{-1}), M is the molecular mass of the analyte (in units of mg mmol^{-1}), and W is the mass of the TiO_2 coating (in units of g). It should be noted that Γ is directly proportional to the (negative) change in frequency, which is the parameter measured by the MERM.

For purposes of comparison, acetone adsorption on the TiO_2-coated magnetic ribbons was also characterized using Fourier transform infrared (FT-IR) spectroscopy in a separate system. A recirculating experimental apparatus was constructed as shown in Figure 6. The overall system consisted of a temperature-controlled chamber, a glass tube packed with four TiO_2-coated magnetic ribbons, stainless steel tubing, a sampling port, a 4.8-m gas sample cell (model 4.8-PA, Infrared Analysis, Inc., Anaheim, CA), a piston pump, and the FT-IR instrument. The interior void volume of the recirculating system was 0.59 L. A similar experimental configuration has been previously reported.[35]

As with the MERM experiments, the foils were preconditioned prior to conducting an adsorption experiment with the FT-IR by heating to 100 °C (in situ) while in the presence of flowing UHP nitrogen; this procedure required opening the recirculating loop. After cooling the foils and closing the loop, acetone was introduced into the system by injecting the liquid form through the sampling port. Gas-phase concentrations were then monitored using a Magna 750 series II FT-IR (Nicolet Instruments, Madison, WI) with a globar source and liquid nitrogen-cooled MCT-A (HgCdTe) detector. The optical path was kept free of ambient CO_2 and water interferences by flowing high-purity preconditioned air (i.e., scrubbed of water vapor and CO_2) through the interior of the spectrometer. All spectra were collected under ambient conditions of temperature and pressure. Single-beam IR spectra were the result of 50 coadded interferograms with a spectral resolution of 1 cm^{-1}. Acetone vapor was quantified using selected infrared absorbance bands that exhibited an adequate linear response (defined as the absorbance area in the region between 1260 and 1160 cm^{-1}). Calibration concentrations were determined by sampling the gas in the FT-IR recirculating system using a gastight syringe and injecting the sample into the gas chromatograph described in the previous section (Hewlett-Packard 5890 series II with FID detection). The concentrations obtained by GC were then used to calibrate the FT-IR response.

Analyte surface concentration (Γ, in units of mmol g^{-1}) for the FT-IR experiments was calculated by difference using the following equation

$$\Gamma = \frac{\left(\frac{V_{\mathrm{injected}} D}{M} - C_{\mathrm{meas}} V_{\mathrm{void}}\right)}{W} \qquad (3)$$

where V_{injected} is the volume of liquid spiked into the system (in units of μL), D is the density of the liquid (in units of mg μL^{-1}), M is the molecular mass (in units of mg mmol^{-1}), C_{meas} is the gas-phase concentration measured by FT-IR (in units of mmol L^{-1}),

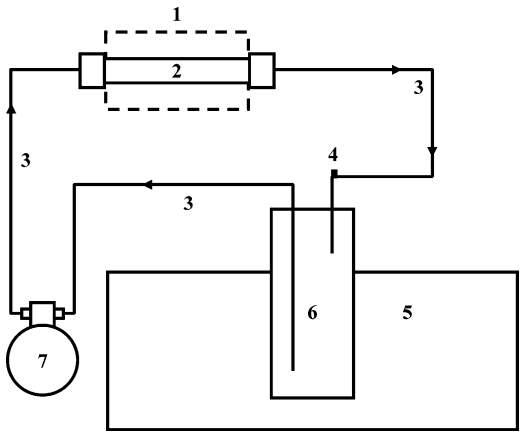

Figure 6. Experimental setup for the FT-IR adsorption measurements. 1, temperature-controlled chamber; 2, glass tube packed with four titanium dioxide-coated magnetic ribbons; 3, stainless steel tubing; 4, sampling port (septum); 5, FT-IR instrument; 6, gas sample cell; and 7, piston pump.

V_{void} is the void volume of the loop (in units of L), and W is the mass of the TiO_2 coating (in units of g). Attempts were made to quantify the adsorption contributed by the interior surfaces of the experimental system by conducting experiments as described above but in the absence of coated ribbons. The methods employed here were not sensitive enough to detect any adsorption by the system components; therefore, their effects are not incorporated into eq 3.

RESULTS AND DISCUSSION

MERM Characterization and Calibration. As described in the Experimental Section, the MERM was initially characterized with respect to reproducibility and day-to-day stability by monitoring the resonant frequency of a representative uncoated ribbon over a period of 9 days (a total of 45 individual measurements were collected). No apparent time trends (i.e., progressively increasing or decreasing resonant frequency) were observed during this experiment. In addition, the observed reproducibility was quite good. The average measured resonant frequency of this ribbon was 54131.9 Hz, with a 95% confidence interval of ±0.7 Hz (or ~1 μg). In a similarly performed study, the resonant frequency of an individual ribbon was found to be independent of gas flow rate in the range of 68−548 mL min^{-1} (i.e., the slope of the regression line was not significantly different from zero; $p = 0.657$).

Calibration of the MERM was accomplished by depositing varying amounts of platinum metal onto several magnetic ribbons, measuring the change in mass (Δm) with an analytical balance, and measuring the change in resonant frequency (Δf) using the MERM. A plot of $-\Delta f$ (where $\Delta f = f$ after coating minus f before coating) as a function of Δm (where $\Delta m = m$ after coating minus m before coating) is shown in Figure 7. As shown, the MERM response is linear through a 1-kHz frequency change, or ~1.5 mg mass change, with a slope of 590.64 Hz mg^{-1} [the intercept of the calibration function is not significantly different from zero ($p = 0.938$)].

The limit of detection (i.e., smallest detectable change in mass) of this device can be estimated by combining the data obtained from the reproducibility study with the calculated calibration parameters. Estimates were made using an MDL (method detec-

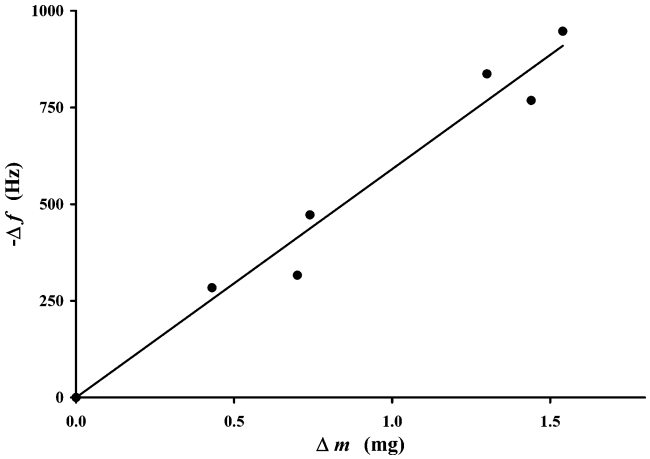

Figure 7. Linear relationship between the change in resonant frequency and the mass of platinum metal deposited onto various magnetic ribbons. Slope = 590.64 Hz mg^{-1}. The intercept of the calibration function is not significantly different from zero ($p = 0.938$).

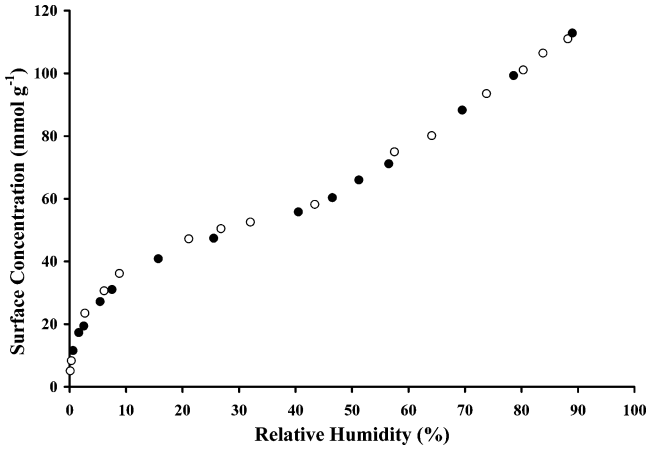

Figure 8. Water adsorption (●) and desorption (○) isotherms on titanium dioxide-coated magnetic foils measured with the magnetoelastic resonance microbalance.

tion limit)-type estimation[38] as well as more rigorous calibration-based methods reported by Zorn et al.[39,40] To calculate Δf values (the MERM instrumental response variable correlated to the change in sensor mass in the previous section) for detection limit estimations, the minimum f of all values in the reproducibility experiment was subtracted from each individual absolute resonant frequency data point. The standard deviation (s) of these Δf values was then calculated. This value of s was then used to calculate an MDL-type detection limit, in which MDL is equal to s times Student's t value corresponding to 99% confidence (one-sided) with $n - 1$ degrees of freedom.[38] The detection limit estimated using this procedure was 7.4 μg, where $s = 3.1$ μg, $n = 45$, and $t_{(44,\ 1-\alpha=0.99)} = 2.414$. Using more statistically rigorous calibration methods,[39,40] the critical level (decision limit that corresponds to the smallest instrument response that is significantly different from zero response) was estimated at 6.0 Hz, and the detection limit (the smallest detectable change in mass) was estimated at 15 μg. It should be noted that rigorous attempts were not made to optimize the MERM for maximum sensitivity. For example, the resolution (or interval between successive data points) was set at 4.0 Hz in these experiments. It is reasonable to expect that simply increasing the number of data points collected within a given frequency range would result in the ability to detect smaller changes in resonant frequency, thereby decreasing the detection limit. More recent work by Zeng et al.[20] with a modified MERM system that was based on frequency counting of the response of a transient excited magnetoelastic sensor reported a measurement resolution of <1.0 Hz.

Adsorption of Water Vapor. Using the experimental setup shown in Figure 4, the adsorption and desorption behavior of water vapor on a TiO_2-coated ribbon was studied. After preconditioning and cooling a coated ribbon, the resonant frequency under dry conditions (UHP nitrogen flowing at 250 mL min^{-1}) was measured. The films used in this study were preconditioned at 100°C; at this temperature, most of the chemisorbed water (H_2O or OH) still remains on the TiO_2 surface. The coated ribbon was exposed to increasing and decreasing water vapor concentrations to create the isotherms shown in Figure 8 (all reported data points are above the estimated limit of detection). Increasing the relative humidity causes new water molecules to adsorb onto the TiO_2 surface by hydrogen bonding to the chemisorbed water (i.e., physisorption). The concentration of water on the TiO_2 surface (Γ) was calculated by measuring Δf at each condition and incorporating this value into eq 2. The relative humidity to which the coated ribbon was exposed was measured using a humidity meter connected at the outlet of the adsorption chamber.

As shown in eq 2, the surface concentration is directly proportional to $-\Delta f$ (the parameter measured by the instrument); therefore, Figure 8 represents a calibration curve for the response of the coated sensor to the gas-phase water concentration. Response of the titania-coated sensor does not follow a simple linear (first-order) calibration function; however, it might be possible to appropriately model the data using a more complex relationship (e.g., a higher order polynomial model). In addition, there are limited regions (e.g., 50−90% RH) that could be modeled using a simple linear function.

The isotherm of Figure 8 has the characteristic features of a type IIa isotherm in the IUPAC classification.[41,42] This type of isotherm is normally associated with monolayer/multilayer adsorption on an open surface (nonporous or macroporous materials); however, it can also account for a limited quantity of micropores.[41] The region of the water adsorption isotherm below 40% relative humidity should account for the filling of micropores in addition to multilayer adsorption on the walls of larger pores. The absence of a sharp point B (knee point) indicates a significant overlap between monolayer and multilayer adsorption. In the multilayer region of a type IIa isotherm, adsorption increases exponentially with increasing partial pressure of adsorbate, explained by capillary condensation when the water vapor pressure inside the pores of the titania equals the saturation vapor

(38) U.S. EPA *Fed. Regist.* **1984**, *49*, 43430−31.
(39) Zorn, M. E.; Gibbons, R. D.; Sonzogni, W. C. *Environ. Sci. Technol.* **1999**, *33*, 2291−95.
(40) Zorn, M. E.; Gibbons, R. D.; Sonzogni, W. C. *Anal. Chem.* **1997**, *69*, 3069−75.
(41) Rouquerol, F.; Rouquerol, J.; Sing, K. *Adsorption by powders and porous solids*; Academic Press: San Diego, CA, 1999.
(42) Sing K. S. W.; Everett, D. H.; Haul R. A. W.; Moscou, L.; Pierotti, R. A.; Rouquerol, J.; Siemieniewska, T. *Pure Appl. Chem.* **1985**, *57*, 603.

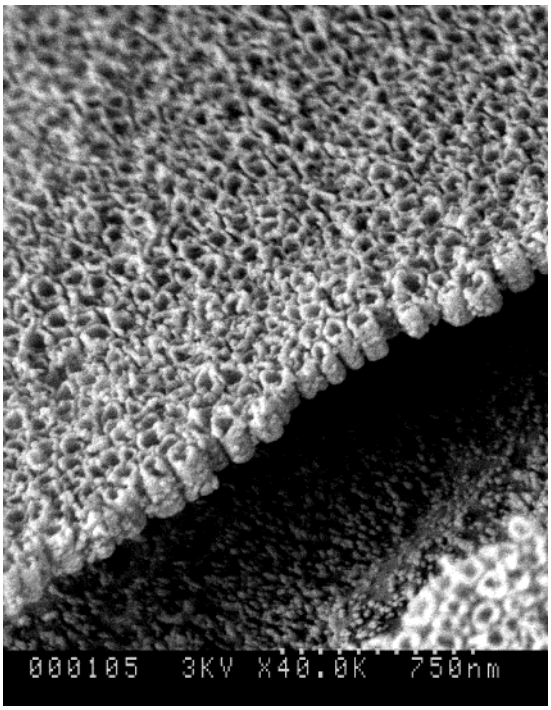

Figure 9. SEM image of a titanium dioxide coating deposited onto a magnetoelastic substrate. The magnification is 40 000×. Specific details of the SEM procedure have been previously reported.[43]

pressure. However, in the isotherm of Figure 8, water adsorption increases linearly with partial pressure in this region (above 50% RH). The large amount of water adsorption by this material in the monolayer region is indicative of a large specific surface area. Thus, the TiO_2 coating should be identified as a porous film, with large external surface area.

Previous publications that utilized similar metal oxide-coated magnetoelastic ribbons have reported the presence of a nanoscale porous honeycomb structure present in the films.[13,43] This type of structure would result in a broad pore size distribution and might explain the adsorption behavior observed in this study above 50% relative humidity. A representative SEM image from these separate studies is shown in Figure 9; specific experimental parameters can be found in Varghese et al.[43] This image shows the presence of a honeycomb structure with pores of ∼76 nm in diameter, which are much larger than the primary particles in the sol, previously reported to be ∼5 nm in diameter.[23] The walls of the structures are likely formed by the coordination of primary particles, having a microporous or small mesoporous structure, and can account for the large water adsorption below 20% relative humidity. These primary aggregates are loosely packed to create an open (honeycomb) overall structure that likely occurs during the coating of the sol onto the magnetic substrate. It is possible that the behavior above 50% relative humidity is a combination of two separate adsorption phenomena. Capillary condensation may be occurring in the interparticle space of the primary aggregates, while at the same time, multilayer adsorption continues to occur on the walls of the larger pores, even at high relative humidity. These overlapping processes may result in a blurring of the distinct capillary condensation shape and the lack of the plateau in the isotherm at higher RH.

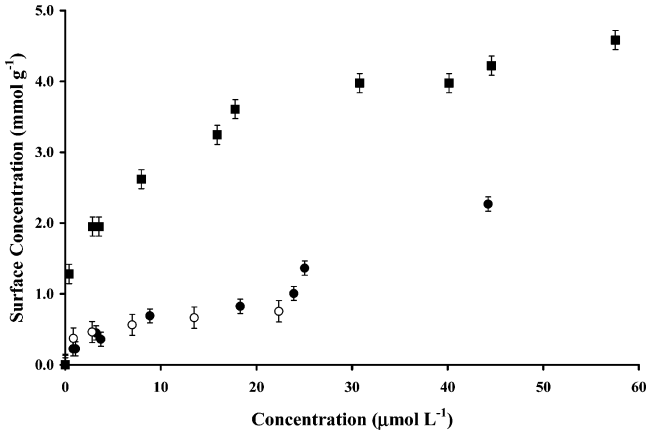

Figure 10. Isopropyl alcohol (■) and acetone (●) adsorption isotherms on titanium dioxide-coated magnetic foils measured with the magnetoelastic resonance microbalance, and acetone adsorption isotherm on titanium dioxide-coated magnetic foils measured with FT-IR (○). [Note: at 1.0 atm and 20.0 °C, 1.0 μmol L^{-1} = 24.1 ppmv.]

Adsorption of Isopropyl Alcohol and Acetone Vapor. Using the experimental setup shown in Figure 4, the adsorption of isopropyl alcohol and acetone vapor on TiO_2-coated ribbons was studied using the MERM. Prior to testing, the coated ribbons were again preconditioned and cooled. The concentration of test compounds on the TiO_2 surface (Γ) was again calculated by measuring Δf at each condition and incorporating this value into eq 2. The gas-phase concentration to which the coated ribbons were exposed was measured by removing subsamples from the gas delivery stream and injecting them into a GC with FID.

MERM adsorption isotherms of isopropyl alcohol and acetone vapor are shown in Figure 10 (as before, all reported data points are above the estimated limit of detection). Errors bars are included in this figure and are estimated on the basis of the MERM reproducibility experiment detailed above. As expected, isopropyl alcohol is adsorbed to a larger extent than acetone as a result of the ability of the alcohol to hydrogen bond with the titania surface.[44,45] Acetone adsorbs less strongly, mainly as a result of weaker dipole interactions with the surface. The monolayer surface concentration is ∼5 times larger for isopropyl alcohol, as compared to acetone. It is more difficult to assess the adsorption behavior of these organics at higher gas phase concentrations because the region of study is somewhat limited; however, it is possible that the open pore structure of these thin films may be altering the adsorption behavior at relatively high analyte concentration.

Since the surface concentration is directly proportional to $-\Delta f$, Figure 10 also represents a calibration curve for the response of the coated sensor to the gas-phase concentration of the two organics. As with water vapor, the titania-coated sensor's response to acetone and isopropyl alcohol does not follow a simple linear (first-order) relationship. Analysis of these compounds would require a calibration function that is more complex than a simple linear model, or application in a somewhat limited concentration range.

(43) Varghese, O. K.; Gong, D. W.; Paulose, M.; Grimes, C. A.; Dickey, E. C. *J. Mater. Res.* **2003**, *18*, 156−65.

(44) Obee, T. N.; Hay, S. O. *J. Adv. Oxid. Technol.* **1999**, *4*, 147−52.

(45) Obee, T. N.; Brown, R. T. *Environ. Sci. Technol.* **1995**, *29*, 1223−31.

Also shown in Figure 10 is the adsorption isotherm determined for acetone using the FT-IR experimental configuration. Error bars are also included for the FT-IR data and are estimated on the basis of separate reproducibility experiments. The acetone isotherm determined with the MERM (which measures adsorption directly as a change in mass) shows excellent agreement with the isotherm determined with the FT-IR configuration (which measures adsorption as the difference between expected and observed gas-phase concentration). This observation suggests that the MERM calibration between the observed change in resonant frequency and the change in mass is valid.

The fact that the MERM calibration for the magnetoelastic ribbons coated only with platinum metal is also valid for the ribbons coated with platinum metal and TiO_2 indicates that the effective Young's modulus of elasticity (Y_{eff}) is the same for both systems ($Y_{eff} = \alpha_c Y_c + \alpha_s Y_s$).[2] This is likely due to the fractional cross section of the coatings (α_c) being small compared with that for the uncoated ribbon (α_s). The other two parameters (Y_c and Y_s) are Young's modulus of the coating and Young's modulus of the uncoated ribbon, respectively. Although this methodology for calibrating the MERM worked fine for the sensors used in this study, it may not be totally applicable to every coated magnetoelastic ribbon.

CONCLUSIONS

A magnetoelastic microbalance (MERM) was used to directly measure the adsorption behavior of gas-phase compounds onto the surface of a porous titanium dioxide thin film. The underlying MERM technique (with an uncoated sensor) showed excellent day-to-day stability, and a linear calibration over a 1-kHz change in frequency, or a 1.5-mg change in mass. Using a 38.1-mm-long × 12.7-mm-wide × 30.5-μm-thick sensor, the MERM system was able to detect a mass change of 15 μg, corresponding to a differential unit area mass loading of 0.016 $\mu g/mm^2$, without any efforts at sensitivity optimization. One interesting feature associated with the technique is that the process of applying the coating on the magnetic ribbons appears to affect the structure of the resulting thin film, resulting in an open honeycomb structure.

ACKNOWLEDGMENT

Support of this work by the National Science Foundation through Grant ECS-0196494 is gratefully acknowledged.

Received for review March 18, 2003. Accepted August 22, 2003.

AC034273Z